Scientific Research

Carbon Doped Nano-Crystalline TiO₂ Photo-Active Thin Film for Solid State Photochemical Solar Cells

Raymond Taziwa, Edson Meyer

Institute of Technology (FHIT), University of Fort Hare, Alice, South Africa
Email: rtaziwa@ufh.ac.za

Abstract

Carbon doped titanium dioxide ($C\text{-}TiO_2$) is considered as a promising photocatalytic material due to its optical absorption extended in the visible region compared to pure TiO_2. However, in the field of photovoltaic's, use of C-doped nano-crystalline titanium dioxide ($C\text{-}TiO_2$) electrodes for light absorption has been considered to be unnecessary so far. In this context, we report here on the use of $C\text{-}TiO_2$ nano-crystalline electrodes in photochemical solar cells devices (PCSC). Carbon doping has reduced the band gap of TiO_2 to 2.41 eV and 2.25 eV with increase in the doping extent for the 9 mM $C\text{-}TiO_2$ and 45 mM $C\text{-}TiO_2$ respectively. The $C\text{-}TiO_2$ electrodes were first used as photo electrodes for solar cells, exhibiting J_{SC} of 1.34651 mA/cm², V_{OC} 0.683 V, FF 50.23% and η 0.46%. for the 9 mM $C\text{-}TiO_2$ and exhibiting J_{SC} of 1.34651 mA/cm², V_{OC} 0.815 V, FF 54.3% and η 0.59% for the 45 mM $C\text{-}TiO_2$. The fabricated solar cell devices have shown an increase in V_{OC} of up to 0.815 V, which is higher than that of 0.7 V for dye sensitized solar cells. The doping of carbon in TiO_2 lattice was closely studied by SEM, XRD, RS and UV-Vis spectroscopy.

Keywords

Carbon Doped TiO₂, Photochemical Solar Cell, Ultrasonic Spray Pyrolysis

1. Introduction

Titanium dioxide (TiO_2) is a typical n-type semiconductor that is extensively used for many applications, such as optical coating [1], gas sensing [2], photo catalysis [3] and more recently its playing a pivotal role in photo chemical solar cells [4]-[7] due to its favorable physical chemical non toxicity, optical electrical properties, good photo activity, as well as long term stability. Photo electrochemical solar cells (PCSC) are the most ambitious

targets in the utilization of solar energy field [6]-[9]. Among the several contestants for photo-anode materials, TiO_2 has been usually adapted as adequate material since it has established best performance compared to other oxide materials. However, the wide spread utilization of TiO_2 is limited by its low absorption of the available suns radiation in the visible region of the solar spectrum (about 3% - 5%) because of the wide band gap 3.2 eV crystalline Anatase phase [9]-[12]. Thus efforts have been made to enhance solar radiation absorption of TiO_2 in the visible region of the solar spectrum by doping with non-metal elements [13]. In dye sensitized solar cells (DSSC), this is being implemented successfully by anchoring low band gap ruthenium dye on to the surface of TiO_2 [14] [15]. But the ruthenium dyes are expensive and unstable in aqueous solutions. DSSCs have been recognized as the leading photovoltaic alternative to the currently dominant silicon-based solar cells [15]. DSSC has drawn considerable interest as an ideal photovoltaic concept for the production of renewable, clean, and affordable energy. High efficiency (up to 12%), low-cost and an eco-friendly fabrication process, transparency, and simplicity are some of the significant advantages offered by DSSCs [15]. In general, manipulation of semiconductor oxides with different morphologies, transition metal doped nano-crystalline TiO_2 and the quest for new dyes are two major strategies explored for enhancing the absorption of incident light and the collection of photo-generated carriers to further improve the overall power conversion efficiency of DSSCs [16]-[18]. To date, however, most efforts have not led to significantly improved photon conversion efficiency of DSSCs. Alternatively visible light active nano-crystalline TiO_2 has been successfully used in photo catalysis [19] more particularly the use of carbon modified TiO_2 nano-crystalline photo anodes has achieved great success with conversion efficiencies of 23%. Carbon modified nano electrodes have been used because of its capability to absorb visible light in the range 400 - 650 nm. In addition C-TiO_2 has been proven to show improved electron gathering transporting behaviour and inhibiting charge recombination as compared to pure un doped TiO_2 nano-electrodes [19].

Use of these types of hybrid nano-crystalline titanium systems in DSSC to supplement light absorption has been considered to be unnecessary so far. Mainly because organic dyes used as solar sensitizers which are mainly Ru (II) complexes have been used to harvest solar radiation [1]. This method increases the range of visible light response effectively. The incident photo current conversion efficiency (IPCE) for the dye absorbed semiconductor is relatively low below 500 nm and above 650 nm. In addition, the use of pure un-doped titanium dioxide nano-crystalline particles which has oxygen deficiency in the crystalline does not help the situation, as it is known that oxygen deficiency can create electron-hole pairs. The oxidising holes are known to react with either the dye and destroy it and or are scavenged by the iodide ions. It is believed that the back reaction and corrosion of nanometals often take place at the nanometal/dye and nanometal/electrolyte interfaces, decreasing the long-time stability of DSSCs [11] [14] [15]. Therefore it reduces the life span of the DSSC. To minimize spectral losses and electron hole recombination we have fabricated a PCSC consisting of a photo anode of carbon doped titanium dioxide (C-TiO_2) to replace the pure undoped TiO_2 anode in the Grätzel type solar cell. A number of PCSCs have been fabricated which have different concentrations of carbon in the photo anodes. These types of photo anodes built with two or more nonmetals have attracted new attention with advantages ranging from improved spectral response, reduced electron hole recombination and amplified electron transport as compared to single type electrodes such pure anatase TiO_2 [5] [19] [20]. The synthesized PCSCs were structurally, morphologically and optically characterized and its photovoltaic properties were evaluated in this work.

2. Experimental

This section outlines the actual experimental procedures involved in the preparation of precursors solution and deposition of nano porous titanium dioxide thin films using ultrasonic spray pyrolysis.

2.1. Synthesis of Pure Un-Doped TiO_2 and C-TiO_2 Nano-Particles

In a synthesis procedure 781.24 µl of titanium tetraisopropoxide (TTIP) were carefully added to a 100 ml beaker containing 60 mls of pH adjusted double distilled water in an ice bath maintained at 0°C. The precursor solution was added drop wise whilst simultaneously stirring to avoid the formation of white precipitates of titanium hydroxides. The prepared solution was then carefully transferred into 250 ml volumetric flask containing 60 mls. of pH adjusted double distilled water in an ice bath. 0.8103 g of oxalic acid dihydrate ($C_2H_2O \cdot 2H_2O$ Fluka) was then added to the volumetric flask and topped up to the mark whilst simultaneously stirring in an ice bath. The precursor solution was then sonicated for 360 minutes prior to ultrasonic spray. This resulted in preparation of a

9 mM Oxalic acid doped titanium dioxide precursor solution which was coded 9_{OA} C-TiO$_2$. Several other precursor solutions of oxalic acid doped solutions were prepared in much the same way, the only difference was the level of dopant and type of dopant as illustrated here **Table 1**.
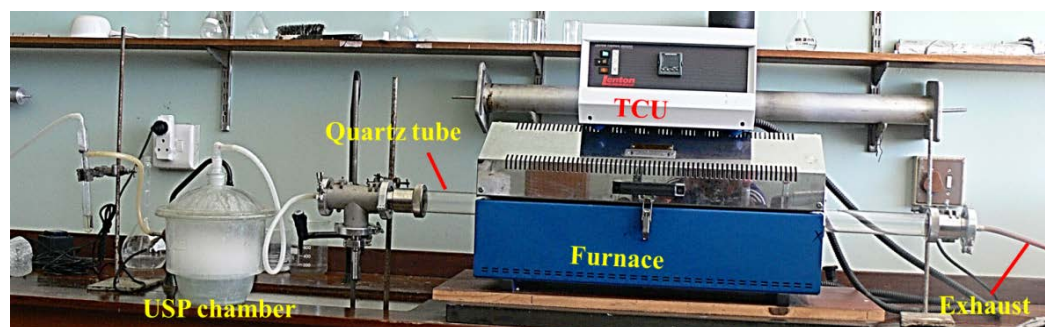
2.2. Ultrasonic Spray Pyrolysis Deposition

In the prepared precursor solution was then decanted into a spray pyrolysis reaction vessels housing a 1.7 MHz ultrasonic nebulizer. Spray deposition begins when vapor of the precursor solution were carried by argon gas at 6 ml/minute into a split tube furnace. The pyrolysis if the precursor resulted in rapid growth of nano-particles which were deposited on fluorine doped tin oxide (FTO) glass substrate. Spray deposition was carried out for 30 minutes and at 450°C. **Figure 1** shows the actual set of the ultrasonic spray pyrolysis employed in the study.

2.3. Characterization

Scanning electron microscopy morphology studies was done using a Jeol JSM-5600 scanning electron microscopy (SEM) microscope which was equipped with an EDX attachement for elemental analysis. X-ray diffraction patterns were gathered using a Philips Xpert powder diffractometer equipped with a CuKα wavelength of 0.154184 nm and graphite crystal monochromator. Survey scans from $2\theta = 20°$ to 80° were performed with a step size of 0.05°. Regional high-resolution XRD scans were also conducted to investigate C-doped TiO$_2$ lattice parameters via the most prominent reflections, using a 0.002° step size. Region 1, from $2\theta = 24°$ - 30°, aimed to capture the anatase (101) and rutile (110) reflections. Region 2, from $2\theta = 35°$ - 43°, examined the A(004), A(112), R(101) and R(111) peaks. Raman spectroscopy was carried out using a Jobin-Yvon T6400 Raman spectrograph operated in triple subtractive mode using, 514.5 nm line. Diffuse reflectance spectra of the resulting nano-powders was obtained using a double beam Lamda 25 Perkin Elemer UV-Vis spectrometer, which was equipped with an intergrating sphere. A given amount of the nano-powder was uniformly pressed in a powder holder (jasco) and placed in the sample holder an intergrated sphere for reflectance measurements. Incident was swept from 100 - 1500 nm. I-V characteristics of the PEC devices were perfomed on a Keithely 2400 source meter under simulated sunlight. I-V and controlled by in house Labview applications. Lamp intestity data was

Table 1. Preperation of oxalic acid (OA) & tetra butyl amonium doped (TBA) TiO$_2$ precursor solutions.

Titanium (IV) isopropoxide (TIP) [1×10^{-2} M]			
Sample Code	Mass of Oxalic Acid (OA) g	Sample Code	Tetra Butyl Ammonium (TBA) (ml) g
9_{OA} C-TiO$_2$	0.8103	9_{TBA} C-TiO$_2$	5.58
18_{OA} C-TiO$_2$	1.6205	18_{TBA} C-TiO$_2$	11.17
27_{OA} C-TiO$_2$	2.4308	27_{TBA} C-TiO$_2$	22.07
36_{OA} C-TiO$_2$	3.2411	36_{TBA} C-TiO$_2$	22.34
45_{OA} C-TiO$_2$	4.05142	45_{TBA} C-TiO$_2$	27.92
54_{OA} C-TiO$_2$	5.66147	54_{TBA} C-TiO$_2$	56.60

Figure 1. It shows actual photo graph of the horizontal ultrasonic spray pyrolysis system utilized in the study.

collected using a Molectron EPM 200 power meter with PM3 thermopile head. Scans were performed under constant power conditions with a 150 W Xe lamp (Oriel). I-V characteristics were at room temperature and were obtained under 1 sun intensity (100 mW/cm^2). A glass filter cuvette filled with water was used as an IR Filter to minimize heating and a UV Filter was used to filter UV bandgap irradiation. The cell was placed in the path of the incident light and scanned from I_{SC} (0 V) to V_{OC} (720 mV) at 68 mV/s with 16 mV increments and 10 point averaging at each increment.

## 2.4. Assembly of Photochemical Solar Cells

To fabricate the PCSCs, two holes were made within 1mm from the edges of FTO platinized electrodes prior to the doctor blading of the pt paste. USP developed working electrodes of C_{OA}-TiO$_2$, C_{TBA}-TiO$_2$ and the platinized counter electrodes were put together in a sandwich configuration using meltonix gasket and hot presser to fabricate a PCSC device as shown here in **Figure 2**. In the sealed configuration the inter-electrode space was filled with I_3^-/I^- redox complex using commercial syringes. The holes created for filling up the electrolyte were then sealed with the aid of small pieces of microscope cover glass slides and meltonix gasket using a soldering gun. To complete the PCSC silver was coated on the edges of each electrode and allowed to dry. Conductive copper was the tapped over the silver contacts. Thus a PCSC device thus fabricated.

3. Results & Discussions

The surface morphology of the as synthesized thin films has been analyzed by SEM. Clearly **Figure 3** reveals that the synthesized thin films for PCSC application have multiple porous network structure. This is prerequisite for PCSC solar cell application. This porous network structure of the thin films allows the redox electrolyte to percolate the entire nano-structure for efficient electron hole regeneration. Also a noteworthy feature in these thin films is that as the carbon dopant level increases from 9 mM C-TiO$_2$ to 18 mM C-TiO$_2$ there shows a distinct change in arrangement of nano-structure. Cauliflower nano-structures develop as illustrated here in **Figure 3(b)**. Inserts in **Figure 3(a)** and **Figure 3(b)** also shows elemental analysis by EDS of the nano-crystalline 9$_{TBA}$ C-TiO$_2$ thin film synthesized on F: SnO$_2$ glass substrates using USP technique has shown the presence titanium (Ti), oxygen (O) and carbon (C). The EDS spectra of the as synthesized thin films also indicate the presence of
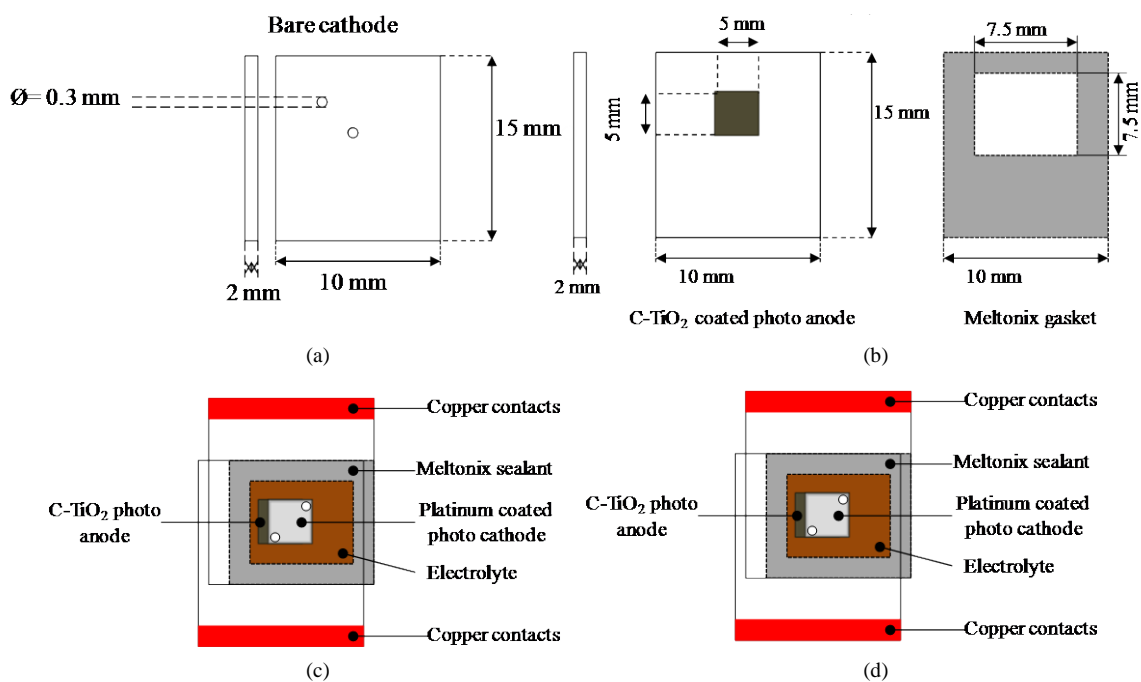
Figure 2. It illustrates the assembly of PCSC starting with (a) drilling of hole on bare photocathode (b) development of platinized photocathode (c) & (d) PCSC device in sealed configuration with redox electrolyte filled in between the inter electrode space.
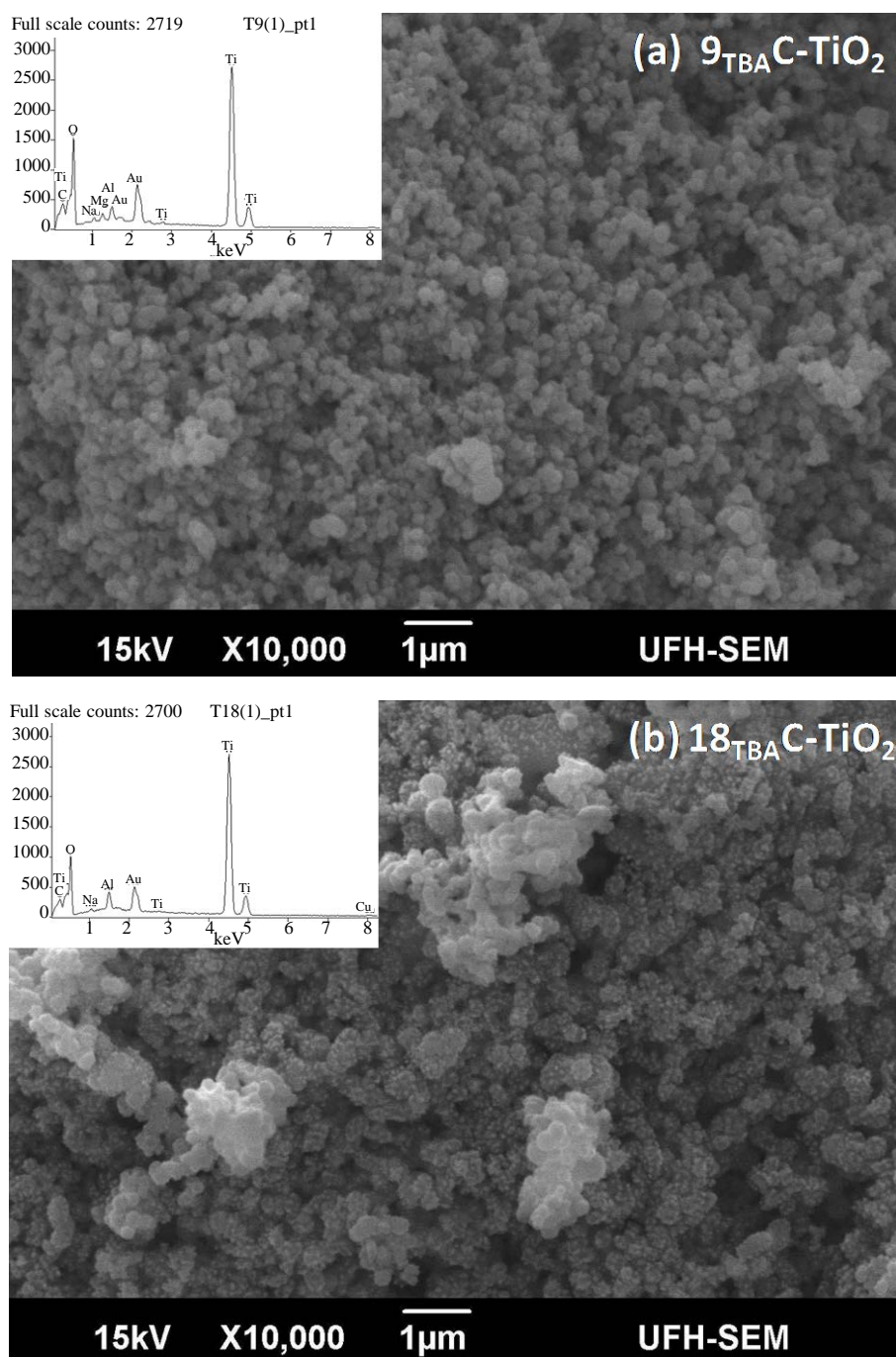
Figure 3. SEM image of surface morphology of nano-crystalline and EDS spectra for (a) $9_{TBA}C\text{-}TiO_2$; (b) $18_{TBA}C\text{-}TiO_2$ thin film.

other elements (*i.e.*) gold (Au) from the gold coating in SEM sample preparation, aluminum (Al) from the aluminum reaction vessel or substrate holders used in the study. Sodium (Na) and magnesium (Mg) originate from the FTO glass substrate. The EDS spectrum also reveals that the titanium atom has different oxidation states. Titanium atom appears at 0.52 KeV, 2.75 KeV, 4.3 KeV and 4.9 KeV. This is due to different binging energies of the core electrons. The first peak of titanium at 0.52 KeV overlapping with oxygen might be due to the high oxidation state of Ti(IV) and other peaks at 4.2, 4.3 & 4.9 KeV are due to titanium in oxidation state of plus three Ti(III). The decline in titanium oxidation state has been ascribed due to carbon doping.

XRD was used to investigate the crystalline structure of TiO_2 samples as well as the structural effects of carbon doping. **Figure 4** shows that the XRD spectra of the as synthesized nano-particles are very broad which indicates large crystallite sizes and/or strain. The synthesized samples showed Anatase TiO_2 as the main polymorph present in the samples. The Anatase peaks are indexed as (101), (004), (200), (105), (211), (116), (220) and (215) in order of increasing diffraction angles. These diffraction angles indicate a body centered tetragonal crystalline structure of TiO_2. The peaks of C-TiO_2 samples were shifted to higher diffraction angles as compared to that of pure un-doped TiO_2 samples by ~0.06. This shift implies that an oxygen atom in the TiO_2 was substituted by a small atom carbon. The recorded XRD patterns were further analyzed with JADE software to determine average particle sizes by use of the Scherer's formula .The analyses revealed that the particle size ranged from 18 - 19 nm which was decreasing with increase in carbon concentration.

Raman spectroscopy was used to analyze the samples and complement XRD results for phase identification. The Rutile phase of TiO_2 is tetragonal and exhibits symmetry characters of the space group D_{4h}^{14} with two TiO_2 formula per unit cell. Four active Raman modes with symmetry B1g (143 cm^{-1}), Eg (447 cm^{-1}), A1$_g$ (612 cm^{-1}) and B$_{2g}$ 826 cm^{-1}. Whilst the Anatase phase has a tetragonal D_{14h}^{19} containing two units per unit cell. According to group theory, there are 6 Raman Active modes with symmetry Eg (143 cm^{-1}), Eg (196 cm^{-1}), B1$_g$ (397 cm^{-1}), doublet (A1g + B1g) 516 cm^{-1} and Eg (640 cm^{-1}). The measured Raman spectrum **Figure 5** shows that the as synthesized nano-particles both for pure un-doped TiO_2 and C-TiO_2 are well crystallized in the Anatase phase of TiO_2. Such a conclusion is in good agreement with the XRD analysis.

It is well known that the photo sensitivity of semiconductors is related to its band gap [21] [22]. The UV-Vis diffuse reflectance spectra of the as synthesized thin films are shown here in **Figure 6**, for comparison the spectrum for un-doped titanium dioxide is also shown.

The 9 mM oxalic acid doped titanium dioxide ($9_{(OA)}$ C-TiO_2) showed a 6 nm shift absorption in visible spectrum with an absorption edge at 402 nm, whilst the $36_{(OA)}$ C-TiO_2, $45_{(OA)}$ C-TiO_2 showed absorption edges at 404 nm and 403 nm respectively. The USP synthesized samples for oxalic acid doped samples for $27_{(OA)}$ C-TiO_2 showed a band gap equal or lower than that of pure un-doped TiO_2 (spectra not shown). The blue shift of the absorption edge observed with $27_{(OA)}$ C-TiO_2 can be attributed to charge transfer transition between the metal ion d electrons and the conduction or valence band of TiO_2 [4]. However the spectra for $18_{(TBA)}$ C-TiO_2 showed showed in **Figure 7** an absorption edge that was red shifted to 495 nm, $36_{(TBA)}$ C-TiO_2 at 512 nm and $45_{(TBA)}$ C-TiO_2 had an absorption edge at 550 nm.
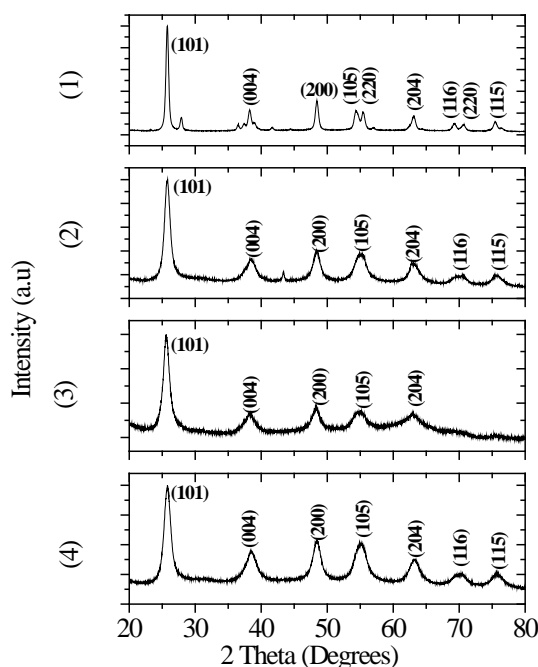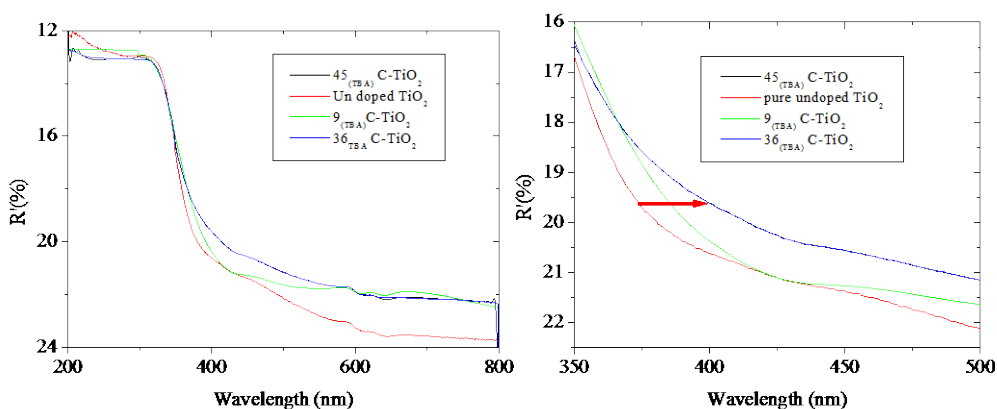

Figure 4. XRD pattern for the as synthesized thin films (1) un doped TiO_2; (2) 9 mM C-TiO_2; (3) 36 mM C-TiO_2, (4) 45 mM C-TiO_2.
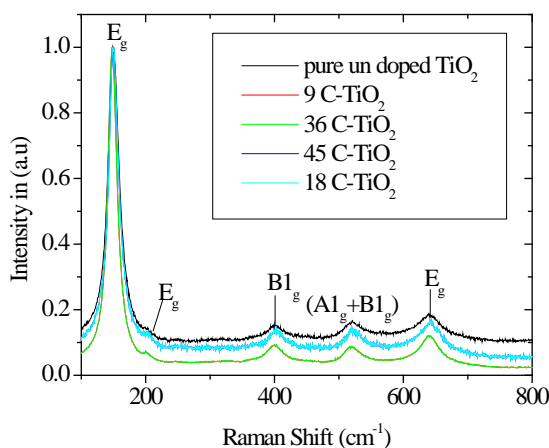
Figure 5. Depicts the Raman spectra for the as synthesized thin films.
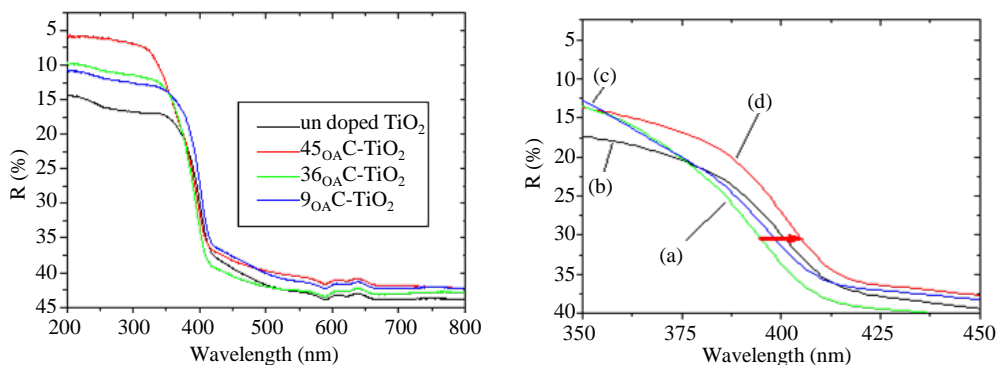
Figure 6. It shows the DRS spectra of the OA doped thin films (a) Un doped TiO_2; (b) $9_{OA}C$-TiO_2; (c) $36_{OA}C$-TiO_2; (d) $45_{OA}C$-TiO_2. Also it shows the extended DRS spectra in the range 350 - 500 nm.

Figure 7. It shows the DRS spectra of the TBA doped thin films Un doped TiO_2, $9_{TBA}C$-TiO_2 $36_{TBA}C$-TiO_2, and $45_{TBA}C$-TiO_2. Also shows the extended DRS spectra in the range 350 - 500 nm.

The samples doped with TBA doped TiO_2 showed an enhanced shift than those of OA. This is mainly because TBA has a higher carbon composition than oxalic acid despite its lower diffusion mobility into the TiO_2 and large molecular size as compared to OA. The enhanced absorption might also be due to the presence of ammonium ion which contains the nitrogen atom in TBA. It is well known that nitrogen doping as compared to carbon doping shows enhanced doping hence a massive shift in the absorption edge. Nitrogen doping has proven more efficient at improving visible light activity. It is theorized that the carbon states are too deep within the band gap

to significantly increase visible light activity, unlike nitrogen doping 1 s state, which successfully overlap with the band O2p states [21]. To establish the type of band gap transition of the as synthesized thin films, the DRS data were fitted to equations for both direct and indirect band gap transitions. The Profiles showed perfect fit for direct band gap transition. The energy band gaps of the thin films were estimated by using Equation (1) in this work. The calculated energy band gaps are presented here in **Table 2** & **Table 3**.

$$Eg = \frac{1239}{\lambda_{edge}} eV \tag{1}$$

where λ_{edge} is the wavelength of the absorption edge.

During the J-V measurement, four parameters such as J_{SC}, V_{OC}, FF and η were obtained of the fabricated PCSCs. **Figure 8** shows the J-V curves for several PCSCs fabricated. An oxalic acid doped photo-electrode (9_{OA} C-TiO$_2$) based in PCSC showed an V_{OC} of 0.682 V, J_{SC} of 1.33201 mA·cm^{-2}, a fill factor of 50.2%, and an efficiency of 0.456%, 9_{TBA} C-TiO$_2$ V_{OC} of 0.683 V, J_{SC} of 1.33465 mA·cm^{-2}, a fill factor of 50.3%, and an efficiency

Table 2. It shows the determined absorption edge λ (nm) and the estimated energy band gap for the OA doped thin films.

Sample Code	Absorption Edge (λ) nm	Energy Band Gap (eV)
9_{OA} C-TiO$_2$	346	3.12
18_{OA} C-TiO$_2$	404	3.06
27_{OA} C-TiO$_2$	396	3.12
36_{OA} C-TiO$_2$	403	3.06
45_{OA} C-TiO$_2$	405	3.05

Table 3. It shows the determined absorption edge λ (nm) and the estimated energy band gap for the TBA doped thin films.

Sample Code	Absorption Edge (λ) nm	Energy Band Gap (eV)
Un doped TiO$_2$	346	3.12
9_{TBA} C-TiO$_2$	496	2.49
36_{TBA} C-TiO$_2$	512	2.41
45_{TBA} C-TiO$_2$	550	2.25
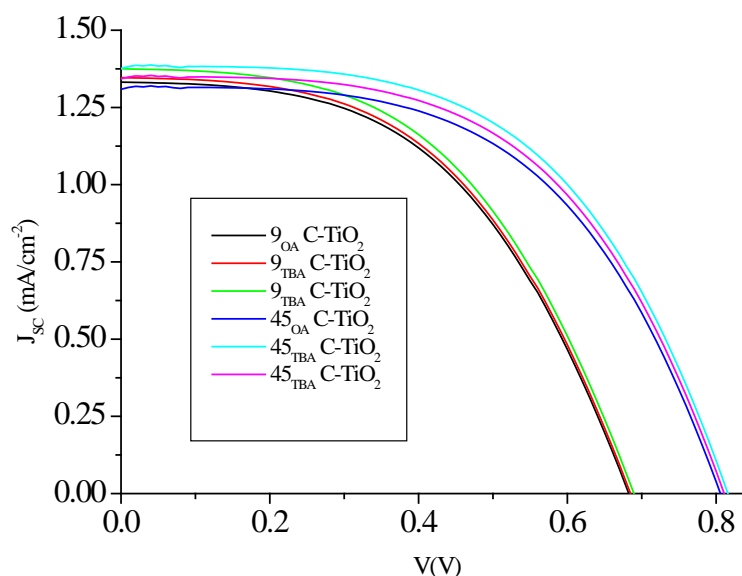
Figure 8. J-V characteristics of the fabricated PCSCs.

of 0.462%. 45_{TBA} C-TiO$_2$ 9 TBA doped photo-electrode showed photo electrode showed a maximum conversion with an open circuit voltage of (V$_{OC}$) of 0.817 V, photocurrent J$_{SC}$ of 1.37639 mA/cm^2, a fill factor of 54.5% and an efficiency of 0.613%. The abrupt increase in J$_{SC}$ by 49% was particularly notable. Light absorption as was noted from the DRS spectra of 9_{OA} C-TiO$_2$ showed an absorption edges around 404 as compared to the TBA doped photo-electrodes which showed an absorption edges at around 551 nm. This increase in photo current generation as the dopant type change might due to (1) increase in (2). The chemical structure of oxalic acid ($C_2O_4^{-2}$) has 27% by mass ratio of carbon as compared to 59% ration of carbon in tetra butyl ammonium ($C_{16}H_{36}BrN$) (3) it has been admitted that the incorporation of C in the nano-structure TiO$_2$ can help fill some oxygen vacancies naturally present in pure un doped titanium leading to reduced trap state distributions and improved charge mobilities [22].

In addition pure un-doped titanium dioxide contains oxygen defects which cause carrier trapping at the surface of pure un-doped TiO$_2$ nano-particles leads to a low electron diffusion coefficient (7×10^{-6} cm$^{-2} \cdot$V$^{-1} \cdot$s^{-1}) [22]. A notable feature of the present results is that the open circuit voltage V$_{OC}$ of the carbon TBA doped electrode (45_{TBA} C-TiO$_2$) is relatively high (0.815 V) about 4% than that of conventional DSSC typically ~0.75 V [8]. According to the kinetic model, the open circuit voltage is given by E$_F$-E$_{redox}$ where EF is the Fermi level of TiO$_2$ and E$_{redox}$ is the redox potential of the electrolyte. The actual V$_{OC}$ obtained in experiments is lower than the theoretical upper limit due to the dark current in a solar cell. The dark current is mainly caused by carrier recombination between the photo injected electrons in the semiconductor and the positively charged electrolyte. Our current studies have shown a higher V$_{OC}$ which indicates that there is lower carrier recombination as compared to conventional DSSC.

4. Conclusion

We have also demonstrated that C-TiO$_2$ nano-structured photo electrodes with optical band gaps in the visible section of the solar spectrum can be obtained with oxalic acid and tetrabutyl ammonium bromide as the carbon sources using spray pyrolysis technique. Our analysis has also shown that the TBA doped samples exhibit a greater shift in absorbance as compared to OA doped sample. The results are evidenced by extended absorption edges of 45_{TBA} C-TiO$_2$ photo electrode which were well above the 500 nm mark. Furthermore the respective solar cells have shown higher conversion efficiencies as compared to the OA doped photo electrodes. The PCSC device with a 45_{TBA} C-TiO$_2$ photo electrode showed the highest solar conversion with an open circuit voltage of (V$_{OC}$) of 0.817 V, photocurrent J$_{SC}$ of 1.37639 mA/cm^2, a fill factor of 54.5% and an efficiency of 0.613%. Admittedly the overall solar cell efficiency for the PCSC devices employing TBA doped titanium dioxide is still very low ~0.6% as compared to the dye sensitized counterpart fabricated by Grätzel in 1991 with an efficiency of ~11%. Therefore, C-doped TiO$_2$ nano-crystals prepared by our approach are ideal semiconductor materials for DSSC and PCSC devices. This study has revealed that our method of fabricating PCSC devices using ultrasonic spray pyrolysis has low cost, simple processing, excellent reproducibility, easy to extend on a large scale production and is applicable in the field of solar energy conversion.

Acknowledgements

References

[1] Markowska-Szczupak, A., Ulfig, K. and Morawski, A.W. (2011) The Application of Titanium Dioxide for Deactivation of Bioparticulates: An Overview. *Catalysis Today*, **169**, 249-257.

[2] Sanchez, M. and Rincon, M.E. (2012) Effect of Multiwalled Carbon Nanotube Functionalization on the Gas Sensing Properties of Carbon Nanotube-Titanium Dioxide Hybrid Materials. *Diamond & Related Materials*, **21**, 1-6. http://dx.doi.org/10.1016/j.diamond.2011.09.010

[3] Ban, Y.X. and Wang, X.C. (2011) Features and Application of Titanium Dioxide Thin Films in Water Treatment. *Procedia Engineering*, **24**, 663-666. http://dx.doi.org/10.1016/j.proeng.2011.11.2714

[4] Chu, D.B., Yuan, X.M., Qin, G.X., Xu, M., Zheng, P., Lu, J. and Zha, L.W. (2008) Efficient Carbon-Doped Nanostructured TiO$_2$ (Anatase) Film for Photoelectrochemical Solar Cells. *Journal of Nanoparticle Research*, **10**, 357-363. http://dx.doi.org/10.1007/s11051-007-9241-7

[5]   Im, J.S., Yun, J., Lee, S.K. and Lee, Y.-S. (2012) *Journal of Alloys and Compounds*, **513**, 573-579.

[6]   Xie, Y.N., Hung, N., Liu, Y.M., Sun, W.W., Mehanane, H.F., You, S.J., Wang, L.Y., Liu, W., Guo, S.S. and Zhao, X.Z. (2013) Photoelectrodes Modification by N Doping for Dye-Sensitized Solar Cells. *Electrochimica Acta*, **93**, 202-206. http://dx.doi.org/10.1016/j.electacta.2013.01.091

[7]   Melhem, H., Simon, P., Wang, J., Di Bin, C., Ratier, B., Leconte, Y., Herlin-Boime, N., Makowska-Janusik, M., Kassiba, A. and Boucle, J. (2012) Direct Photocurrent Generation from Nitrogen Doped TiO_2 Electrodes in Solid-State Dye-Sensitized Solar Cells: Towards Optically-Active Metal Oxides for Photovoltaic Applications. *Solar Energy Materials & Solar Cells*, **117**, 624-631.

[8]   Murayama, M. and Mori, T.T. (2008) Novel Tandem Cell Structure of Dye-Sensitized Solar Cell for Improvement in Photocurrent. *Thin Solid Films*, **516**, 2716-2722. http://dx.doi.org/10.1016/j.tsf.2007.04.076

[9]   Nosaka, Y. (2011) Comprehensive Nanoscience and Technology. *Solar Cells and Photo Catalysis*, **1**, 571-605.

[10]   Nagaveni, K., Hegde, M.S., Ravishankar, N., Subbana, G.N. and Madras, G. (2004) Synthesis and Structure of Nanocrystalline TiO_2 with Lower Band Gap Showing High Photocatalytic Activity. *Langmuir*, **20**, 2900-2907. http://dx.doi.org/10.1021/la035777v

[11]   Cong, Y., Li, X.K., Qin, Y., Dong, Z.J., Yuan, G.M., Cui, Z.W. and Lai, X.J. (2011) Carbon-Doped TiO_2 Coating on Multiwalled Carbon Nanotubes with Higher Visible Light Photocatalytic Activity. *Applied Catalysis B*: *Environmental*, **107**, 128-134. http://dx.doi.org/10.1016/j.apcatb.2011.07.005

[12]   Lee, H.U., Lee, S.C., Choi, S., Son, B., Lee, S.M. and Lee, H.J.K.J. (2013) Efficient Visible-Light Induced Photocatalysis on Nanoporous Nitrogen-Doped Titanium Dioxide Catalysts. *Chemical Engineering Journal*, **228**, 756-764. http://dx.doi.org/10.1016/j.cej.2013.05.059

[13]   Yella, A., Lee, H.W., Tsao, H.N., Yi, C., Chandiran, A.K., Diau, E.W., Yeh, C.Y., Zakeerudin, S.M. and Gratzel, M. (2011) Porphyrin Sensitized Solar Cells with Cobalt (II/III)-Based Redox Electrolyte Exceed 12 Percent Efficiency. *Science*, **85**, 1172-1178.

[14]   Grätzel, M. (2004) Conversion of Sunlight to Electric Power by Nanocrystalline Dye-Sensitized Solar Cells. *Journal of Photochemistry and Photobiology A*: *Chemistry*, **164**, 3-7. http://dx.doi.org/10.1016/j.jphotochem.2004.02.023

[15]   Grätzel, M. (2005) Solar Energy Conversion by Dye-Sensitized Photovoltaic Cells. *Inorganic Chemistry*, **44**, 20-25. http://dx.doi.org/10.1021/ic0508371

[16]   Kubo, W., Sakamoto, A., Wada, T.K.Y. and Yanagida, S. (2004) Dye Sensitized Solar Cells Improvement by Tandem Structure. *Journal of Photochemistry and Photobiology A*: *Chemistry*, **164**, 33-39. http://dx.doi.org/10.1016/j.jphotochem.2004.01.024

[17]   Qin, C.J., Islam, A. and Han, L.Y. (2012) Panchromatic Donor-Acceptor-Acceptor Sensitizers Based on 4H-Cyclopenta[2,1-b:3,4-b']Dithiophen-4-One as a Strong Acceptor for Dye-Sensitized Solar Cells. *Dyes and Pigments*, **94**, 553-556. http://dx.doi.org/10.1016/j.dyepig.2012.03.002

[18]   Bozic-Weber, B., Edwin, C.C. and Housecroft, C.E. (2013) Light Harvesting with Earth Abundant d-Block Metals: Development of Sensitizers in Dye-Sensitized Solar Cells (DSCs). *Coordination Chemistry Reviews*, **257**, 3089-3106. http://dx.doi.org/10.1016/j.ccr.2013.05.019

[19]   Hoffmann, M.R., Martin, S.T., Choi, W. and Bahnemann, D.W. (1995) Environmental Applications of Semiconductor Photocatalysis. *Chemical Reviews*, **95**, 69-96. http://dx.doi.org/10.1021/cr00033a004

[20]   Guo, W., Shen, Y.H., Boschloo, G., Hagfield, A. and Ma, T. (2011) Influence of Nitrogen Dopants on N Doped TiO_2 Electrode and Their Applications in Dye Sensitized Solar Cells. *Electrochemica Acta*, **56**, 4611-4617. http://dx.doi.org/10.1016/j.electacta.2011.02.091

[21]   Castro, A.L., Nune, M.R., Carvalho, M.D., Ferreira, L.P., Jumas, J.C., *et al.* (2009) Doped Titanium Dioxide Nanocrystalline Powders with High Photocatalytic Activity. *Journal of Solid State Chemistry*, **182**, 1838-1845. http://dx.doi.org/10.1016/j.jssc.2009.04.020

[22]   Djerdji, I., Acron, D., Jaglicic, Z. and Niederberger, M. (2008) Nonaqueous Synthesis of Metal Oxide Nanoparticles: Short Review and Doped Titanium Dioxide as Case Study for the Preparation of Transition Metal-Doped Oxide Nanoparticles. *Journal of Solid State Chemistry*, **181**, 1571-1581. http://dx.doi.org/10.1016/j.jssc.2008.04.016